

Article

# Comparative Study about Dimensional Accuracy and Surface Finish of Constant-Breadth Cams Manufactured by FFF and CNC Milling

Enrique E. Zayas-Figueras <sup>\*,†</sup> and Irene Buj-Corral <sup>\*,†</sup>

Department of Mechanical Engineering, Barcelona School of Industrial Engineering (ETSEIB),  
Universitat Politècnica de Catalunya (UPC), Av. Diagonal, 647, 08028 Barcelona, Spain

\* Correspondence: enrique.zayas@upc.edu (E.E.Z.-F.); irene.buj@upc.edu (I.B.-C.);

Tel.: +34-934-01-65-78 (E.E.Z.-F.); +34-934-05-40-15 (I.B.-C.)

† These authors contributed equally to this work.

**Abstract:** In this work, the design, manufacture and measurement process of constant-breadth cams is presented. The motion law of the cam was designed by means of Bézier curves and the corresponding design desmodromic constraints. The cams were manufactured in two different materials employing two different processes: PLA cams with fused filament fabrication (FFF) and aluminium cams with computer numerical control (CNC) milling. The main aim of this work is to compare both types of cams regarding dimensional accuracy and surface finish, in order to evaluate if it would be possible to temporarily replace a metallic cam with a plastic one during the repair of the first one. Dimensions were measured with micrometres and surface roughness with a contact roughness meter. The results show that, in diametral dimensions, similar dimensional error values were obtained for both the 3D-printed and the machined cams. However, in longitudinal dimensions, whose direction is perpendicular to the 3D-printed layers, the 3D-printed cams showed higher dimensional error than the machined ones. The average roughness  $R_a$  in the 3D-printed cams was 20 times higher than in the milled cams. According to the results, it would be recommended to temporarily replace metallic cams with plastic ones in applications of low-power transmission. Given that in the literature little information is available about the measurement of 3D-printed desmodromic cams, this work will contribute to the study and analysis of this kind of 3D printed mechanism.

**Keywords:** constant-breadth cam; design process; FFF; CNC milling; dimensional accuracy; surface finish

**Citation:** Zayas-Figueras, E.E.; Buj-Corral, I. Comparative Study about Dimensional Accuracy and Surface Finish of Constant-Breadth Cams Manufactured by FFF and CNC Milling. *Micromachines* **2023**, *14*, 377. <https://doi.org/10.3390/mi14020377>

Academic Editors: Laurentiu Slatineanu and Adelina Hrițuc

Received: 2 December 2022

Revised: 23 January 2023

Accepted: 26 January 2023

Published: 2 February 2023



**Copyright:** © 2023 by the authors. Licensee MDPI, Basel, Switzerland. This article is an open access article distributed under the terms and conditions of the Creative Commons Attribution (CC BY) license (<http://creativecommons.org/licenses/by/4.0/>).

## 1. Introduction

Desmodromic cam mechanisms use two upper conjugate pairs (geometric closure of the upper pairs) in such a way that both impose the same kinematic restriction, guaranteeing global bilaterality: the loss of contact in one of the pairs is prevented by the other pair. There are four types of planar desmodromic cam mechanisms: (a) constant-breadth cam mechanism, (b) constant-diameter cam mechanism, (c) conjugate cam mechanism and (d) slotted-face cam mechanism (Figure 1). These types of mechanisms are used in different industries such as textile, automotive, etc. Figure 2 shows a photograph of a constant-breadth cam mechanism employed in a traditional sewing machine.

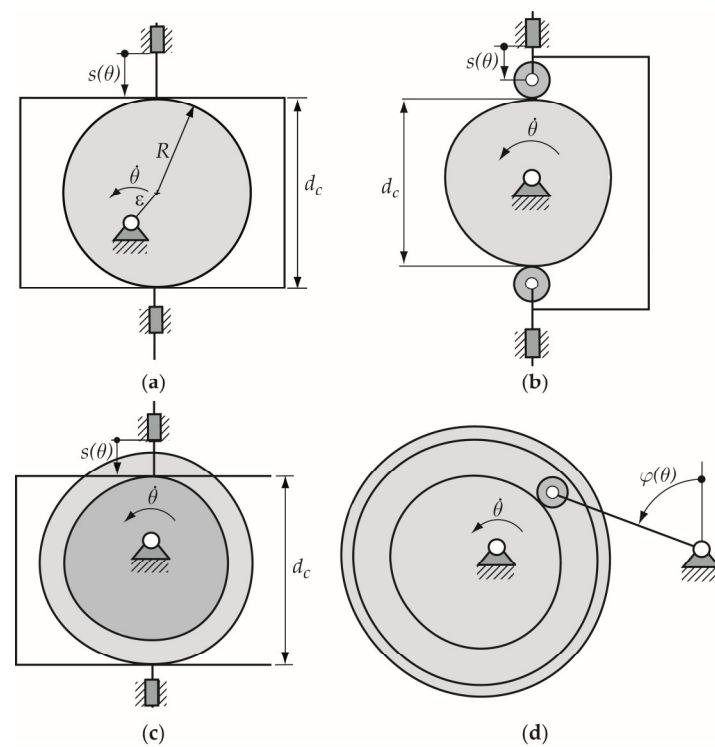


**Figure 1.** Types of planar desmodromic cam mechanisms: (a) constant-breadth cam; (b) constant-diameter cam; (c) conjugate cams; and (d) slotted cam mechanisms, respectively.



**Figure 2.** Photograph of the constant-breadth cam mechanism with a flat-faced double-oscillating follower, used in a traditional sewing machine.

In the case of constant-breadth cam mechanisms, here exposed, the geometry of both cam and follower guarantees the closure of the higher kinematic pairs formed by the bilateral contact of both parts; and this fact implies the precise design and manufacture of the profile of both the cam and the follower. The constant-breadth cams may either be circular arc cams or have arbitrary geometry [1]. An eccentric cam that drives a parallel flat-faced double follower (Figure 1a) can be considered the simplest example of a constant-breadth cam, due its profile being a circumference of radius  $R$ . In this mechanism, the diameter  $2R$  of the eccentric cam coincides with the constant distance  $d_c$  between the two parallel flat surfaces of the follower [2]. The double follower can have a translating or oscillating movement; nevertheless, the displacement function of the follower that guarantees obtaining the corresponding constant-breath cam profile is subject to certain restrictions and consists of two segments: the first one called the designed segment, and the second, which is calculated from the designed segment, called the calculated segment [2–4].

The design process of a cam follower mechanism regarding the geometric and kinematics aspects once the starting design parameters have been chosen consists of three stages: the first stage, the design or synthesis of the follower displacement function—also

known as displacement law; the second stage, obtaining the cam profile that corresponds to the motion law before it is obtained; and the third stage, verifying the correctness of the cam profile geometry by means of evaluating its radius of curvature to avoid an incorrect contact between the cam and the follower. In a previous study [4] conducted by one of the present study's co-authors, the direct synthesis method of a constant-breadth cam mechanism with a parallel flat-faced double-translating follower was presented, showing numerical examples. The design process used in the present work is based on this method.

The methodology used in the present work consists of three main parts: (1) the cam–follower mechanism design process; (2) the manufacturing processes employed to obtain the constant-breadth cam profile by filament fused fabrication (FFF) and numerical control milling processes; and (3) the measurement of the cam profiles obtained—dimensional errors and surface finishing. The mentioned methodology was applied to a constant-breadth cam mechanism that drives a translating flat-faced double follower. In the first part of the methodology—the design process—once the designer agrees with the cam profile obtained in 2D (two dimensions), a 3D (three dimensions) virtual model of the cam–follower mechanism is obtained using computer aided design (CAD) software, where a simulation of the performance of the mechanism is carried out. Later, a prototype of the mechanism is obtained using the additive manufacturing process above mentioned; the physical parts available are checked and later measured. This kind of mechanism is very important to measure the dimensional errors and the surface finish of the cam, and a principal dimension to be checked is the breadth of the cam  $d_c$  (Figure 1a).

The usual manufacturing methods for cams include forging, casting, milling, etc. For example, Lugosi et al. [5] assembled forged powder cams to a shaft by brazing, in order to obtain a camshaft. Luis Perez et al. [6] studied the wear of magnesium aluminium alloy isothermally forged cams. They found a better performance in cams subjected to equal channel angular pressing (ECAP). Nowadays, camshafts are obtained in nodular iron by computer numerical control (CNC) [7]. Forged steel camshafts allow higher loads than cast ones. However, they require subsequent machining processes such as deep drilling to reduce their weight. An alternative way to reduce weight consists of using composite camshafts, which are composed of two different materials and, subsequently, assembled. Typically, a steel tube is used in which the forged cams are assembled: for example, with a shrink fit. In recent years, the lost foam-casting process has been used to produce steel camshafts with hollow shapes that are lighter than the conventional ones. The final machining stage of a camshaft is often a grinding process [8]. In a previous work, the authors of the present paper manufactured flank cams by milling and electro discharge machining (EDM). EDM has the advantage of enabling parts in different conductive materials to be obtained [9]. Some authors have obtained and applied cam–follower mechanisms through additive manufacturing; for example, Cheng et al. [10,11] evaluate the kinematic performance of a desmodromic cam mechanism (a particular type of mechanism that they called composite cam–follower mechanism) that is used to obtain personalized automata. Another application of the 3D-printed cam–follower mechanism is a micro-cam-actuated linear peristaltic pump for microfluidic applications, presented by Xiang et al. [12]. Almeida et al. [13] present the design and modelling of a 3D-printed flexure-based actuation mechanism for robotic microtweezers. The key component is a uniquely designed cam flexure system 3D printed in nylon, which linearly translates the bending of a piezoelectric bimorph actuator into angular displacement. The authors stated that 3D printing made it possible to manufacture the cam with a specifically calculated curve, which would otherwise have been costly using conventional milling techniques.

Different methods are used to measure the dimensions of cams, which can be divided into two groups: non-contact methods (reflection, laser interferometry, electromagnetic induction) and mechanical contact methods [14]. As for non-contact methods, for example, vision machines are used to measure the cam distance in camshafts [15]. A laser sensor is often employed to measure complex shapes, such as those of the cams [16]. In another example about the fabrication of complex shapes, such as those of dental prostheses, Jeong

et al. [17] used the DLP (digital light processing) additive manufacturing process and the CNC milling process to compare the dimensional accuracy achieved by both methods. The prostheses, made of dental resin, were measured by laser scanning, and it was observed that the error of the CNC fabricated parts was higher than that of the DLP printed parts. On the other hand, electromagnetic induction, for instance, is used to determine the angular rotation of rotative components such as gears [18]. A typical contact measuring device for cams is the five-axis coordinate measuring machine [19]. However, conventional measurement tools can also be employed for the same purpose [20].

In the literature, there is little information about the dimensional accuracy and surface finish of 3D-printed cams. In the present work, both the dimensions and roughness values of constant-breadth cams are presented. They were manufactured using both the fused filament fabrication (FFF) and the milling processes. The main reason for the comparison is the possibility of temporarily replacing the metallic cams with those made of PLA obtained by FFF, while the metallic ones are repaired in mechanisms that have more of a kinematic type of operation than high-power transmission. Moreover, the 3D-printed cam–follower mechanism can also be used in scale models in the field of engineering education.

## 2. Materials and Methods

The cam mechanism exposed in this work is a constant-breadth cam with a double flat-faced translating follower, whose geometric parameters are presented in Figure 3. Thus, this section introduces the design process applied to obtain and verify the adequate constant-breadth cam profile, from which the 3D model of the cam is obtained. The manufacturing and measuring processes are also explained.

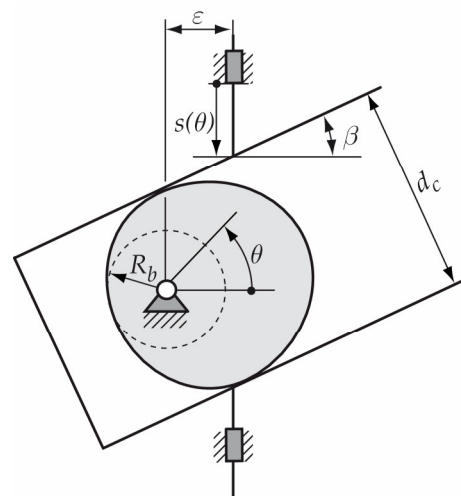


**Figure 3.** Geometric parameters in a constant-breadth cam mechanism:  $R_b$ , radius of the base circle of the cam;  $\epsilon$ , offset of the follower;  $\beta$ , inclination angle of the translating follower; and  $d_c$ , the breadth of the cam.

### 2.1. Design Process of the Cam–Follower Mechanism

Once the designer has chosen the type of cam mechanism to be designed (a constant-breadth cam with a double flat-faced translating follower), the starting data for the design process must be established. These data are: (a) the radius  $R_b$  of the base circle of the cam; (b) the breadth of the cam  $d_c$ , which coincides with the distance between the two parallel flat surfaces of the follower; (c) the offset  $\epsilon$  of the translating follower; and (d) the inclination angle  $\beta$  of the translating follower (Figure 3). Table 1 shows the values of the data here used.

**Table 1.** Geometric parameters chosen for the design of the cam–follower mechanism.

Geometric Parameter [Units]	Numerical Value
Radius of the base circle of the cam $R_b$ [mm]	17.5
Breadth of the cam $d_c$ [mm]	50
Offset of the translating follower $\varepsilon$ [mm]	0
Inclination angle of the translating follower $\beta$ [°]	0

In a cam–follower mechanism the cam drives the follower according to the desired follower displacement law:  $s(\theta)$ , as a function of the angle  $\theta$  rotated by the cam. The design sequence of the cam mechanism, as mentioned in Section 1, consists of the following steps that are explained for the particular case here exposed [2,4].

1. *Designing the displacement law  $s(\theta)$ .* The designer defines the displacement law of the follower according to the movement required by the technological process or function that must be met by the mechanism. As mentioned in Section 1, the displacement law for this particular type of constant-breadth cam mechanism with a double-translating follower must meet a design restriction (expression 1) [2–4]. Thus,  $s(\theta)$  consists of two segments: the designed segment and the calculated segment.

$$s(\theta) + s(\theta + 180^\circ) = \text{constant} = d_c \quad (1)$$

In the case here exposed, the design segment is defined in the interval  $\theta \in [0, 180^\circ]$  using a non-parametric Bézier curve with continuity  $C^3$ , and it comprises one dwell event during  $30^\circ$  of cam rotation and one rise event from  $30^\circ$  to  $180^\circ$ . The desired follower maximum displacement  $s_{max}(\theta)$  is 15 mm. The use of free software, called QtCAM [21], is used to support the design process. For the calculated segment in which  $\theta \in [180^\circ, 360^\circ]$ , it is synthesized according to the process exposed in [4], as well as consisted of two events: an upper dwell of the follower while the cam rotated from  $180^\circ$  to  $210^\circ$ , and a fall event until completion of the entire cycle,  $360^\circ$ . Figure 4a shows the entire displacement law  $s(\theta)$  obtained and its corresponding derivatives: the first is the velocity function  $V(\theta)$  (Figure 4b), the second is the acceleration function  $A(\theta)$  (Figure 4c) and the third is the jerk  $J(\theta)$  (Figure 4d), which allows the designer to make decisions regarding the process design. This guarantees the good performance of the mechanism. In the graphs (Figure 4), the corresponding events of motion are drawn in different colours, with green corresponding to the calculated segment.

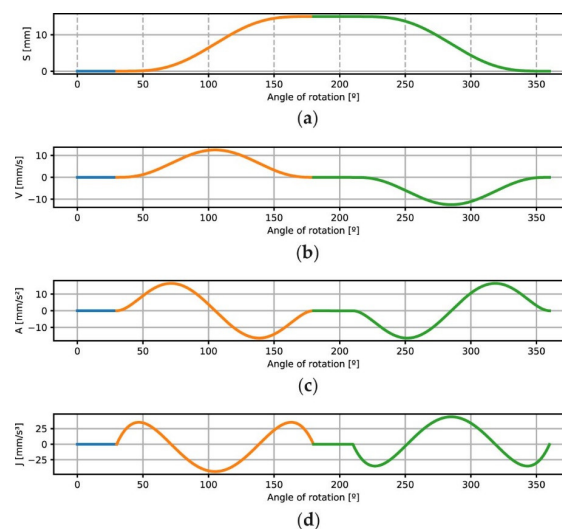


**Figure 4.** (a) The designed displacement law  $s(\theta)$  and its derivatives: (b) the velocity curve  $V(\theta)$ , (c) the acceleration curve  $A(\theta)$  and (d) the jerk curve  $J(\theta)$ .

2. *Obtaining the cam profile* that drives a certain type of follower according to the designed displacement law.

The method applied to obtain the cam profile is based on the proposal of Zayas [22], in which a constant-breadth cam is obtained from the method of generating a mechanism of conjugated cams (Figure 5), where each of them has contact with the flat faces of the double-translating follower; the first cam contacts with the upper point  $P_1$ , and the second cam contacts with the lower point  $P_2$ . The two conjugated cams must have the same geometry and the same orientation, so that they coincide and overlap to represent a single cam of constant breadth  $d_c$  between the parallel faces of the double follower. The profiles of the conjugate cams are obtained from the parametric expressions (2), (3), (4) and (5). The analytic–vectorial method to obtain the cam profile is based on a kinematic inversion, in which two coordinate systems are used, one  $(x, y)$  in which the cam is fixed, and the other  $(1, 2)$  fixed and oriented according to the follower guide (Figure 5).

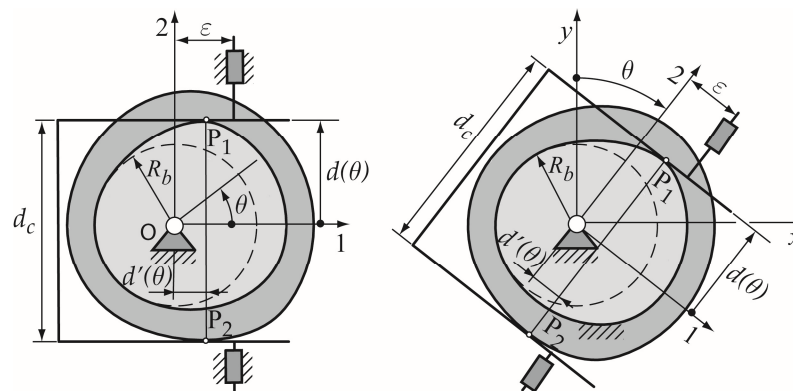


**Figure 5.** Conjugate cam mechanism and its kinematics inversion.

The parametric expressions of the position vectors of the contact points  $P_1$  and  $P_2$  in the mobile base 1, 2 (Figure 5) are the expressions (2) and (3), and in the fixed base  $x, y$  are the expressions (4) and (5); these last expressions are required to obtain the cam profiles.

$$\{\overline{OP_1}(\theta)\}_{1,2} = \begin{Bmatrix} d'_1(\theta) \\ d_1(\theta) \end{Bmatrix}_{1,2}, \quad d_1(\theta) = d_o + s(\theta) \quad (2)$$

$$\{\overline{OP_2}(\theta)\}_{1,2} = \begin{Bmatrix} d'_2(\theta) \\ d_2(\theta) \end{Bmatrix}_{1,2}, \quad d_2(\theta) = (d_o - d_c) + s(\theta) \quad (3)$$

$$\{\overline{OP_1}(\theta)\}_{x,y} = [S_\theta] \begin{Bmatrix} d'_1(\theta) \\ d_1(\theta) \end{Bmatrix}_{1,2}, \quad [S_\theta] = \begin{bmatrix} \cos \theta & \sin \theta \\ -\sin \theta & \cos \theta \end{bmatrix} \quad (4)$$

$$\{\overline{OP_2}(\theta)\}_{x,y} = [S_\theta] \begin{Bmatrix} d'_2(\theta) \\ d_2(\theta) \end{Bmatrix}_{1,2} \quad (5)$$

In expressions (2) and (3), the term  $d_o$  is the minimum distance between the follower and the centre of rotation of the cam up to the point where the follower starts to move. In expressions (4) and (5),  $[S_\theta]$  is the rotation matrix.

Thus, to obtain a constant-breadth cam profile, in addition to the requirement of displacement law (expression (1)), another design constraint must be met, which is that the value of the constant-breadth cam  $d_c$  should be [2,4,21]:

$$d_c = 2R_b + s_{max}(\theta) \quad (6)$$

Figure 6 depicts the constant-breadth cam profile obtained for the case here shown with the parameters shown in Table 1 and the displacement law exposed in Figure 4.

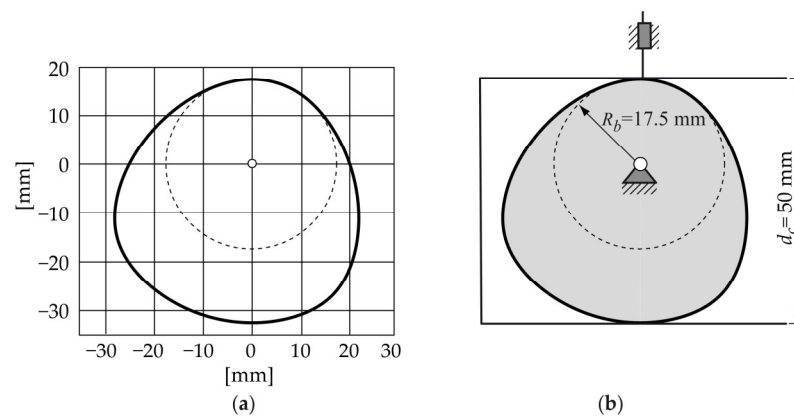


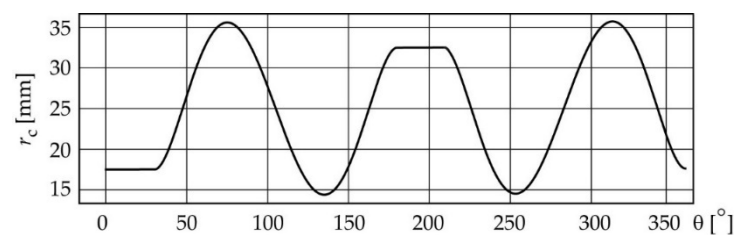
**Figure 6.** (a) Cam profile obtained, (b) constant-breadth cam mechanism.

Once the cam profile is obtained, the third step of the design process is as follows.

3. Verifying that the cam profile obtained does not present geometric characteristics that prevent the right contact between the cam and follower. In the case here exposed, the curvature radii  $r_c$  of the cam profile must always be positive, in order to guarantee correct contact between the cam and the follower. The expression to calculate  $r_c$  is as follows [1]:

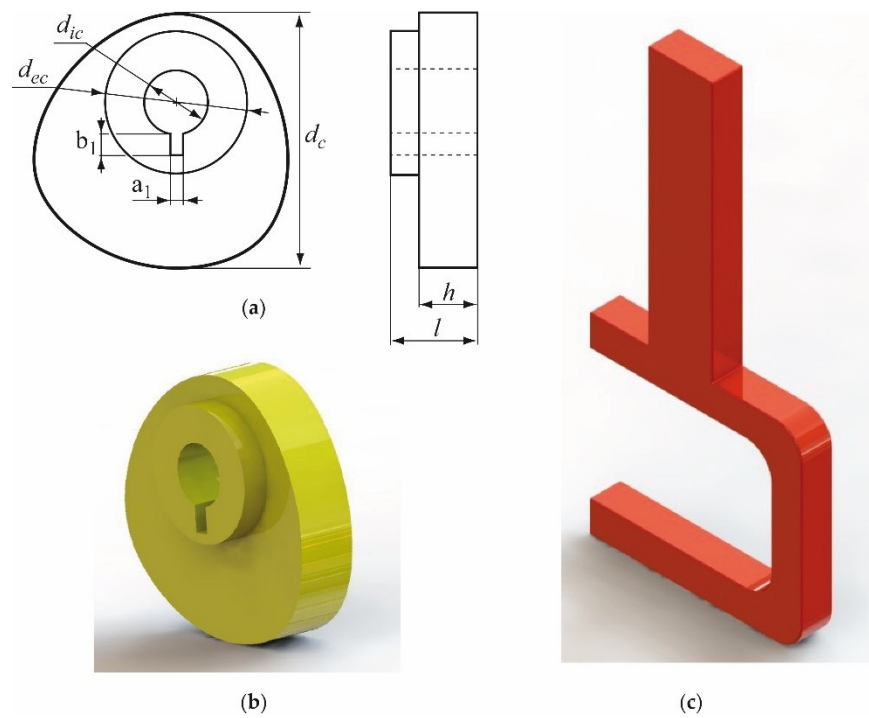
$$r_c(\theta) = (s(\theta) + s_{\theta\theta}(\theta)) \cos \beta - \varepsilon \sin \beta \quad (7)$$

Figure 7 shows the graphics of the curvature radii  $r_c$  corresponding to the constant-breadth cam profile obtained (Figure 6).



**Figure 7.** Curvature radii  $r_c$  of the cam profile with  $\varepsilon = 0$  and  $\beta = 0$ .

In this particular case, the inclination angle of the translating follower is  $\beta = 0$  (Table 1). This angle coincides with the pressure angle, which is an index of the quality of the mechanism; therefore, it is equal to zero, which is an advantage for the dynamic performance of the mechanism because the force exerted by the cam to drive the follower is always vertical. Thus, the next design step is to obtain the 3D virtual design of the cam–follower mechanism and to validate the design. Some additional geometrical dimensions (theoretical dimensions) shown in Figure 8a are defined to obtain the 3D virtual model of the cam. These dimensions are: the internal and external diameters of the hub of the cam  $d_{ic} = 12$  mm and  $d_{ec} = 26$  mm, respectively; the dimensions of the keyway,  $a_1 = 3$  mm and  $b_1 = 5.19$  mm; the width of the working face of the cam,  $h = 12$  mm; and the total length of the cam,  $l = 15$  mm. These values were defined, taking as a reference the dimensions of the shaft where the cam was to be placed. Using the CAD software SolidWorks, 3D virtual models were created of all the parts of the mechanism (the cam (Figure 8b), the follower (Figure 8c), the shaft of the cam, the frame of the mechanism, etc.).



**Figure 8.** (a) Main dimensions of the hub and keyway of the cam, and virtual models of the (b) constant-breadth cam and (c) the double flat-faced follower.

Figure 9 depicts the assembly of the cam–follower mechanism, and Figure 10 shows the curve of the follower displacement obtained by means of the module motion of SolidWorks. The mentioned curve was obtained for several operating cycles, and it can be seen that, for a single work cycle, the events of the follower motion consist of two dwell segments, a rise segment and a fall segment, which coincide with the program of the motion law that was designed (Figure 4a), thus validating the correctness of the design.

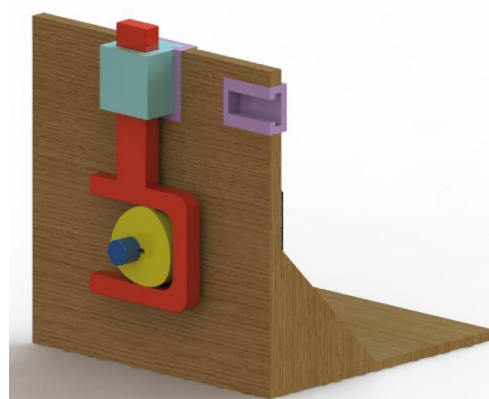


**Figure 9.** A virtual model of the assembled cam–follower mechanism.

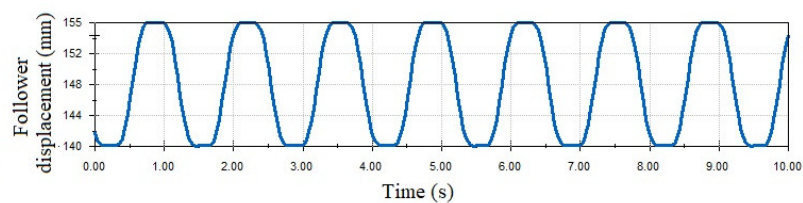


**Figure 10.** Follower displacement function, for several operating cycles, obtained with the motion module of SolidWorks.



Once the constant-breadth cam–follower mechanism design is considered correct, the next step is to manufacture the parts of this mechanism, to measure and check them, as well as to perform the assembly of the mechanism. Following this, the manufacturing process is presented.

## 2.2. Manufacturing Processes of the Cams

The designed cams were manufactured following an additive manufacturing process (3D printing) to obtain the prototypes and, as well as the milling process, to obtain the metal cams.

### 2.2.1. Manufacturing Processes of the 3D-Printed Cams

The 3D-printed cams were obtained using the fused deposition modelling (FDM) or fused filament fabrication (FFF) technique. An Ultimaker 2+ machine was employed, with a 2.85 mm diameter polylactic acid (PLA) filament from the manufacturer RS PRO (particularly the material with RS code 832-0270). The main printing parameters, which were established by employing the slicer software Ultimaker Cura, are summarized in Table 2.

**Table 2.** Main 3D-printing parameters for the cams.

Parameter [Units]	Numerical Value
Nozzle diameter [mm]	0.4
Infill ratio [%]	18
Print speed [mm/s]	60
Infill pattern	Linear
Shell thickness [mm]	0.4
Layer height [mm]	0.15
Printing head temperature [°C]	200
Build plate temperature [°C]	60
Raster angle [°]	45
Number of wall lines	3

Figure 11 shows an image of the cams while being printed on the bed of the Ultimaker 2+ printer. These parts are the prototypes of the cams, which are measured later.

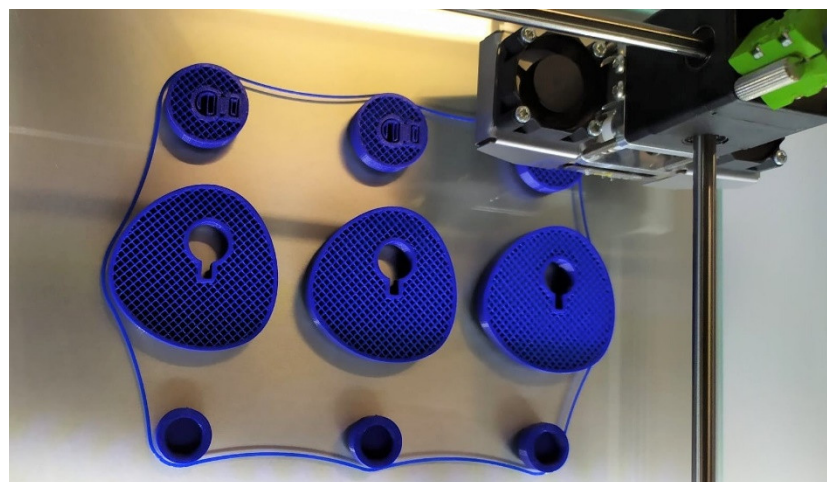


**Figure 11.** Constant-breadth cams being printed on the bed of the printer Ultimaker 2+.

### 2.2.2. CNC Milling of the Cams

Once the prototypes of the cam were validated, it was decided to manufacture three metallic cams through the CNC milling process. First, using the 3D model of the cam

obtained with the CAD SolidWorks, a manufacturing simulation process was carried out by means of the CAD-CAM software Cimatron 11 from Cimatech [23]. This simulation process allowed to validate the machining strategies, the tools and the machining parameters to be used, as well as the corresponding G-code to be used in the Hass VM2 3-axis machining centre. The metal cams were obtained from an aluminium block. Figure 12 shows the sequence of steps followed for the manufacturing process of the cams. It should be noticed that the last image of this figure is an example of the constant-breadth cam obtained by CNC milling.

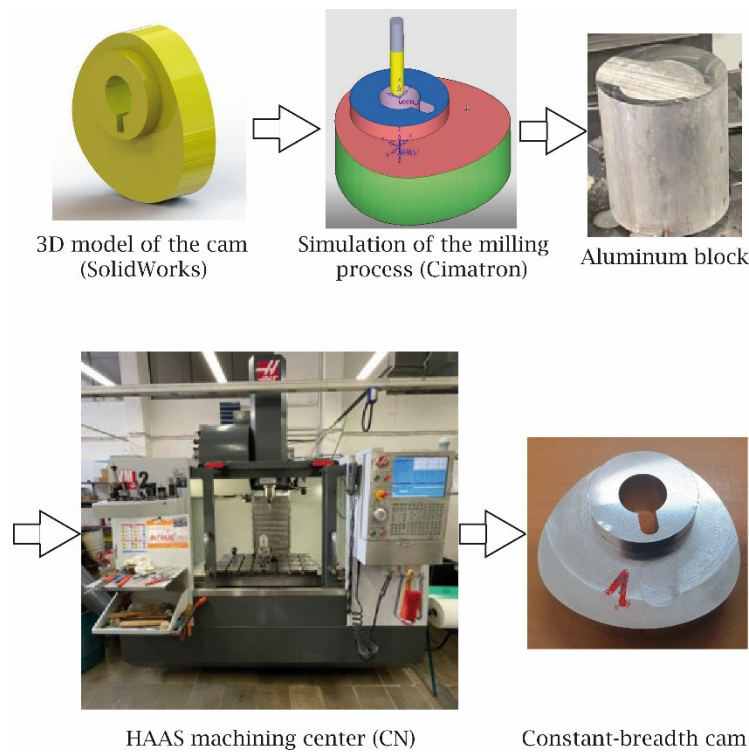


**Figure 12.** The sequence of steps followed to manufacture the metallic cams.

Different machining phases were required, such as: (1) Cutting off of the starting cylinder (aluminium block 6082, with a purity of 96%). (2) Face milling; contouring of the hub; contouring the cam profile; marking, drilling and keyway slotting. (3) Cutting off the contoured cam to define its thickness. (4) Face milling of the lower surface of the cam, leaving a total length of 17.40 mm. (5) Manual filing of the cam edges, removing any sharp edges. Table 3 shows the tools, fixture system and cutting conditions employed to obtain the metallic cams. The dimensions of the keyway and the length of the hub were modified to adapt them to the tools available in the workshop.

**Table 3.** Characteristics of the machining operations to obtain the metal cams.

Operation Number	Operation (Machine Tool)	Tool	Fixture System	Cutting Conditions
1	Cutting off of the starting cylinder (band saw machine)	Band saw	Bench vice	Cutting speed: 30 m/min
2	Face milling (CNC machine centre)	Face milling tool of diameter 40 mm and z = 8	Bench vice	Cutting speed: 150 m/min; feed speed: 955 mm/min; depth of cut: 2 mm

3	Rough contour milling of the cam hub (CNC machine centre)	Face milling tool of diameter 25 mm and $z = 4$	Bench vice	Cutting speed: 120 m/min; feed speed: 611 mm/min; depth of cut: 5.40 mm
4	Rough contour milling of the cam profile (CNC machine centre)	Face milling tool of diameter 25 mm and $z = 4$	Bench vice	Cutting speed: 120 m/min; feed speed: 611 mm/min; depth of cut: 20 mm
5	Marking of the cam hole (CNC machine centre)	Drilling tool of angle $90^\circ$ and diameter 12 mm and $z = 2$	Bench vice	Cutting speed: 95 m/min; feed speed: 302 mm/min; depth of cut: 5 mm
6	Drilling of the cam hole (CNC machine centre)	Drilling tool of angle $120^\circ$ and diameter 12 mm and $z = 2$	Bench vice	Cutting speed: 95 m/min; feed speed: 302 mm/min; cutting length: 22 mm
7	Contour milling of the keyway of $6 \times 4.36$ mm (CNC machine centre)	Face milling tool of diameter 4 mm and $z = 2$	Bench vice	Cutting speed: 120 m/min; feed speed: 1910 mm/min; depth of cut: 22 mm
8	Contour milling of the cam profile (CNC machine centre)	Face milling tool of diameter 10 mm and $z = 4$	Bench vice	Cutting speed: 120 m/min; feed speed: 1528 mm/min; depth of cut: 15 mm
9	Contour milling of the cam's hub (CNC machine centre)	Face milling tool of diameter 10 mm and $z = 4$	Bench vice	Cutting speed: 120 m/min; feed speed: 1528 mm/min; depth of cut: 5.40 mm
10	Cutting off the machined cylinder (band saw machine)	Band saw	Bench vice	Cutting speed: 30 m/min
11	Face milling to final length of the cam of 17.40 mm, obtaining a width of the working face of 12 mm (CNC machine centre)	Face milling tool of diameter 40 mm and $z = 8$	Bench vice	Cutting speed: 150 m/min; feed speed: 955 mm/min; depth of cut: 2 mm

### 2.3. Measuring Process of the Cams

The dimensional measurements of both the 3D-printed and the machined cams were carried out with a conventional disk flange outside micrometre, with a range of 25–50 mm and a precision of 0.01 mm. Figure 13 shows a measuring example for a metallic cam. Three measurements were carried out on each cam, in the three directions indicated with yellow dotted lines in the figure. It should be noticed that parallel micrometre discs (also indicated in yellow colour) are always tangent to the cam profile.

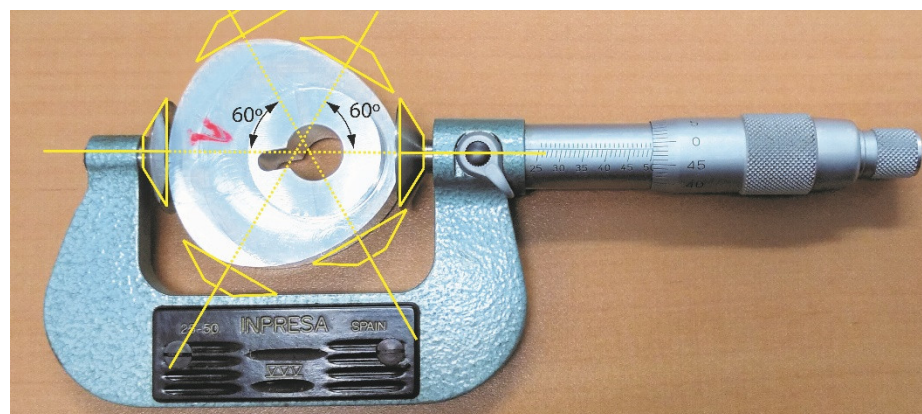


**Figure 13.** Dimensional measurement of the machined cams using a flange outside micrometre, and measuring directions.

The relative error ( $RE$ ) is calculated as follows:

$$RE (\%) = \left[ \frac{\text{Measured value} - \text{Theoretical value}}{\text{Theoretical value}} \right] \cdot 100 \quad (8)$$

The surface roughness of the working face of the cam that is in contact with the follower was measured with a Taylor Hobson Talysurf v2 contact roughness meter, using a Gaussian filter with a cut-off value of 0.8 mm. The 3D-printed and metallic cams were measured by means of the same process. Three measurements were taken on each cam—each one in a different area of the working face, in the longitudinal direction. Figure 14 depicts the case of a machined cam.

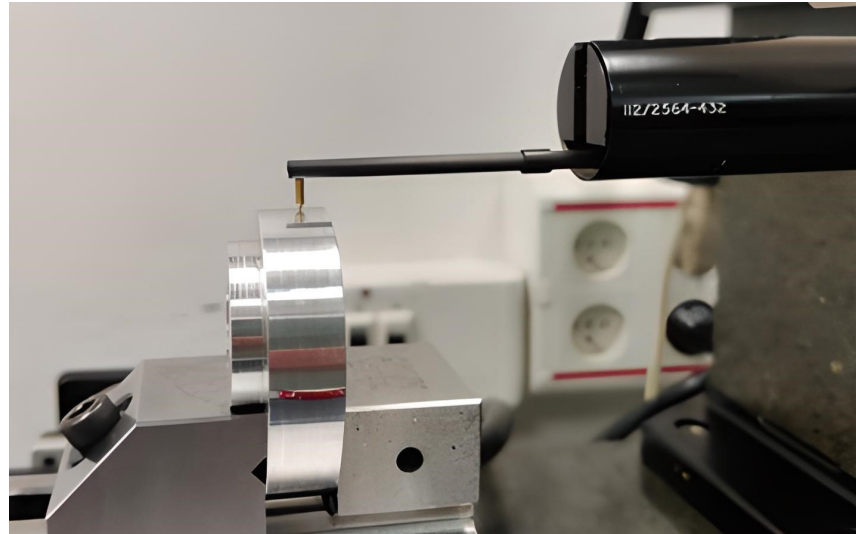


**Figure 14.** Roughness measurement of the working face of a machined cam.

### 3. Results

In the following subsections, the results for the dimensions and roughness of the cams are presented.

#### 3.1. Dimensions

The dimensions of both the 3D-printed and the machined cams are presented in Table 4. It should be noticed that the design parameter constant-breadth  $d_c$  of the cam is the principal dimension (Figure 8), which determines the proper assembly and correct operation of this type of mechanism.

**Table 4.** Dimensions of the 3D-printed and machined cams.

Cam Manufacturing Process	Parameter	Theoretical Value (mm)	Mean Value (mm)	Standard Deviation (mm)	Relative Error (%)
3D-printed	$d_c$	50	49.98	0.06	0.12
	$d_{ic}$	12	11.91	0.05	0.75
	$l$	15	15.17	0.01	1.16
	$h$	12	12.20	0.01	1.64
Machined	$d_c$	50	49.99	0.06	0.07
	$d_{ic}$	12	11.97	0.01	0.30
	$h$	12	11.99	0.09	0.08

Table 4 shows that a similar relative error is obtained in the 3D-printing process and the machining process when diametral dimensions, for example,  $d_c$  and  $d_{ic}$ , are considered

(which depends on  $x$  and  $y$  axes in the printing machine). However, when the  $z$  dimension is considered—for example, in this case the parameters  $l$  and  $h$ —a much higher error is obtained in the 3D-printing process than in the machining process. This can be attributed to the fact that, in the 3D-printed cams, the  $z$  dimension greatly depends on the conditions in which the subsequent layers are deposited. The layer height is one of the main printing parameters influencing surface roughness. In this case, the value of this parameter used for printing the cams was 0.15 mm (Table 2).

### 3.2. Surface Roughness

Figure 15 shows two examples of roughness profile graphs and the corresponding values of the surface roughness measurements, for both the 3D-printed cam (Figure 15a) and the milled cam (Figure 15b), respectively. Table 5 contains the  $R_a$  values, as well as the standard deviation, for both the 3D-printed and the machined cams.

**Table 5.** Average surface roughness  $R_a$  for the 3D-printed and machined cams.

Cam Manufacturing Process	Mean Value [ $\mu\text{m}$ ]	Standard Deviation [ $\mu\text{m}$ ]
3D-printed cams	10.41	0.12
Machined cams	0.50	0.03

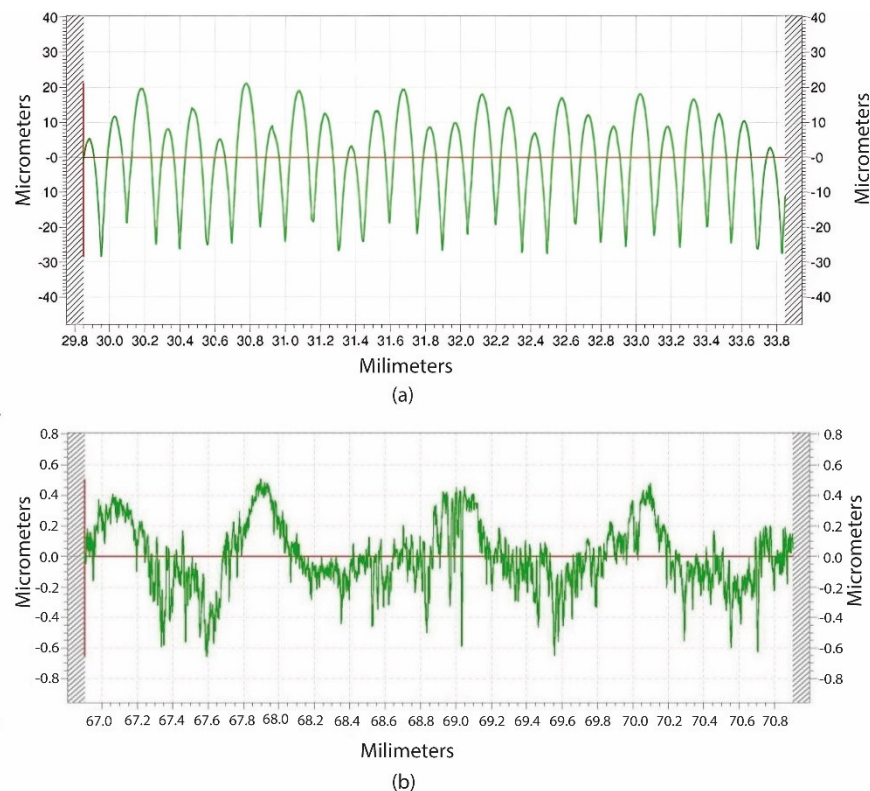


**Figure 15.** Roughness profile graphs of (a) a printed cam and (b) a milled cam.

As mentioned in Section 2.3, roughness was measured along the longitudinal direction of the cam, which corresponds to a generatrix of the working face of the cam. From Figure 15a, it can be seen that the 3D-printed cam has a regular roughness profile, with rounded peaks and sharp valleys, in which each peak corresponds to a printed layer. On the contrary, from Figure 15b it is observed that, for the machined cam, a more irregular profile is obtained along the machined furrow. This is usual when a side milling operation is employed [24]. Only small peaks and valleys are detected, corresponding to slight machining marks.

By analysing the results shown in Table 5, the  $R_a$  values for the machined cams were 20 times lower than for the 3D-printed ones. It is well known that, in FFF processes, high surface roughness is obtained in lateral walls, which are perpendicular to the deposition plane of the layers [25]. Similar  $R_a$  values up to  $0.41 \mu\text{m}$  were previously reported in machined flank cams [9].

#### 4. Discussion

The relative error values achieved in this work for 3D-printed cams are similar to those obtained for 3D-printed gears in PLA material in the  $xy$  plane (below 0.8 %) [26]. These errors are of the same order of magnitude as the relative errors of the machined parts. However, higher relative errors of up to 1.64% were obtained for 3D-printed cams in the Z direction, which is perpendicular to the deposition plane of the parts. Beniak et al. [27] found that high layer height and high printing temperature led to lower dimensional accuracy in 3D-printed parts. Pennington et al. [28] observed that part size and printing temperature influenced dimensional accuracy in 3D-printed parts. It is not only the 3D printing parameters that influence dimensional accuracy, but also other parameters such as the material type, the material composition and the part geometry [29]. To reduce the dimensional error of PLA-printed parts containing cylindrical holes, Popescu et al. proposed using a high layer height of 0.32 mm, three shells and a high printing speed of 65 mm/s as the 3D printing parameters [30].

As for the requirements regarding dimensional accuracy in metallic cams, Rothbart [31] defined, in a milled and ground cam, an accuracy of  $\pm 0.0254 \text{ mm}$  for an approximate diameter of 300 mm in a cylindrical cam. In this work, a higher value of  $\pm 0.06 \text{ mm}$  is reported, considering only the milling operation.

Although in this work the cams were manufactured by means of milling operations and no grinding was carried out, average roughness  $R_a$  was approximately 20 times lower for the machined parts than for the 3D printed ones. This highlights one of the main disadvantages of the FFF technology, due to the fact that the parts are manufactured layer-by-layer [27]. In FFF processes, roughness mainly depends on the selected layer height. Although this parameter could be reduced, it is limited and the quality of the parts. Specifically, the dimensional accuracy would worsen if a too low layer height value were selected [32]. In the case here presented, a value of 0.15 mm was used, providing a good quality of the 3D printed cams. Galantucci et al. [33] reported that roughness depends on nozzle diameter, raster width and layer height. Hartcher-O'Brien et al. [34] found that low layer height and low print speed favour low surface roughness.

Regarding metallic cams, the required surface finish is  $R_a < 0.4 \mu\text{m}$  [35]. This often implies a subsequent grinding operation [36]. In aluminium machined cams, Veera et al. [37] reported  $R_a$  values around  $1 \mu\text{m}$ , which are higher than those obtained in this work. For structural steel flank cams, lower  $R_a$  values below  $0.3 \mu\text{m}$  were reported [9].

According to the results in the present work, and considering the dimensional accuracy, it would be possible to replace metallic cams with plastic ones in mechanisms that have more of a kinematic type of operation than of high-power transmission. On the other hand, for that kind of mechanism, the surface finish is a less significant influential factor regarding the proper operation of the mechanism.

#### 5. Conclusions

In the present work, constant-breadth cams were designed, manufactured and measured. In the design process, the QtCAM software was used to obtain and verify the cam profile, and the SolidWorks software was used to create the virtual model of the cam-follower mechanism and validate its correct operation. Regarding the design process, the main conclusion is:

- Two principal design desmodromic constraints must be considered in the design process of a constant-breadth cam that drives a double flat-translating follower. The first

constraint is that the motion law  $s(\theta)$  consists of two segments: the designed segment, which can only be designed in the interval from 0 to 180° of cam rotation), and the calculated segment, which is obtained using the expression 1. The second constraint is that the value of the constant-breadth cam  $d_c$  is equal to the diameter of the base circle plus the maximum displacement of the cam follower.

In the manufacture of the cams, two different processes were used: extrusion 3D printing utilizing the fused filament fabrication (FFF) technology and CNC machining. Both the dimensions and the surface finish of the cams were measured. The main conclusions are as follows:

- Similar dimensional relative errors were obtained for the 3D-printed cams and the machined parts when the  $x$ ,  $y$  plane was considered (maximum relative error of 0.75%). However, when the  $z$  direction was considered, which is orthogonal to the depositing plane of the printed layers, higher dimensional relative errors were reported for the 3D-printed cams (up to 1.64%) than for the machined ones (up to 0.54%);
- As for the surface finish on the lateral surface (working face) of the cams, the average roughness  $R_a$  was around 20 times higher for the 3D-printed cams (10.41  $\mu\text{m}$ ) than for the machined ones (0.50  $\mu\text{m}$ ).

According to the results obtained in this work, it would be possible to temporarily replace metallic cams with plastic ones in mechanisms that have more of a kinematic type of operation than of high-power transmission. Little information is available about the dimensional accuracy and surface finish of 3D-printed desmodromic cams. Thus, this work will contribute to the study and analysis of this kind of mechanism.

**Author Contributions:** Conceptualization: E.E.Z.-F. and I.B.-C. Methodology: E.E.Z.-F. and I.B.-C. Software: E.E.Z.-F. and I.B.-C. Validation: E.E.Z.-F. and I.B.-C. Formal analysis: I.B.-C. and E.E.Z.-F. Investigation: I.B.-C. and E.E.Z.-F. Resources: I.B.-C. and E.E.Z.-F. Data curation: I.B.-C. and E.E.Z.-F. Writing—original draft: E.E.Z.-F. and I.B.-C. Writing—review and editing: E.E.Z.-F. and I.B.-C. Visualization: E.E.Z.-F. and I.B.-C. Supervision: I.B.-C. and E.E.Z.-F. Project administration, I.B.-C. and E.E.Z.-F. Funding acquisition, I.B.-C. All authors have read and agreed to the published version of the manuscript.

**Funding:** This research received no external funding.

**Data Availability Statement:** Data are available upon request.

**Acknowledgments:** The authors would like to thank Alejandro Domínguez, Ramón Casado, and Alberto Rodero for their help with the experimental tests. This research did not receive any specific grant from funding agencies in the public, commercial, or not-for-profit sectors.

**Conflicts of Interest:** Enrique Ernesto Zayas-Figueras and Irene Buj Corral report a relationship with the Polytechnic University of Catalonia (UPC) that includes employment and non-financial support. The UPC had no role in the design of the study; in the collection, analyses, or interpretation of data; in the writing of the manuscript; or in the decision to publish the results.

## References

1. Cardona, S.; Zayas, E.E.; Jordi, L. Radius of curvature and sliding velocity in constant-breadth cam mechanisms. *Mech. Mach. Theory* **2014**, *81*, 181–192.
2. Zayas, E.E.; Cardona, S.; Jordi, L. Analysis and synthesis of the displacement function of the follower in constant-breadth cam mechanisms. *Mech. Mach. Theory* **2009**, *44*, 1938–1949.
3. Ye, Z.; Smith, M.R. Synthesis of constant-breadth cam mechanisms. *Mech. Mach. Theory* **2002**, *37*, 941–953.
4. Cardona, S.; Zayas, E.E.; Jordi, L.; Català, P. Synthesis of displacement functions by Bézier curves in constant-breadth cams with parallel flat-faced double translating and oscillating followers. *Mech. Mach. Theory* **2013**, *62*, 51–62.
5. Lugosi, R.; Brauer, M.; Cook, J. Assembled camshaft for I.C. engines with forged powder metal cams. *SAE Trans.* **1987**, *96*, 455–465.
6. Luis Pérez, C.J.; Luri Irigoyen, R.; Fuertes Bonel, J.P.; León Iriarte, J.; Salcedo Pérez, D.; Puertas Arbizu, I. Experimental and fem analysis of wear behaviour in AA5083 ultrafine-grained cams. *Metals* **2020**, *10*, 479.

7. Röhrle, M.D. The camshaft in the course of time. *MTZ Worldw.* **2002**, *63*, 7–9.
8. Liu, T.; Deng, Z.; Luo, C.; Li, Z.; Lv, L.; Zhuo, R. Chatter detection in camshaft high-speed grinding process based on VMD parametric optimization. *Meas. J. Int. Meas. Confed.* **2022**, *187*, 110133.
9. Buj-Corral, I.; Zayas-Figueras, E.; Montaña-Faiget, À. Comparative study of flank cams manufactured by wedm and milling processes. *Metals* **2020**, *10*, 1159.
10. Cheng, Y.; Sun, Y.; Song, P.; Liu, L. Spatial-temporal motion control via composite cam-follower mechanisms. *ACM Trans. Graph.* **2021**, *40*, 1–15.
11. Cheng, Y.; Song, P.; Lu, Y.; Chew, W.J.J.; Liu, L. Exact 3D Path Generation via 3D Cam-Linkage Mechanisms. *ACM Trans. Graph.* **2022**, *41*, 1–13.
12. Xiang, J.; Cai, Z.; Zhang, Y.; Wang, W. A micro-cam actuated linear peristaltic pump for microfluidic applications. *Sens. Actuators A Phys.* **2016**, *251*, 20–25.
13. Almeida, A.; Andrews, G.; Jaiswal, D.; Hoshino, K. The Actuation Mechanism of 3D Printed Flexure-Based Robotic Microtweezers. *Micromachines* **2019**, *10*, 470.
14. Liu, Y.; Zhou, H.; Zhao, D.; Guan, X.; Li, G.; Feng, F. Online approach to measuring relative location of spatial geometric features of long rotating parts. *Meas. J. Int. Meas. Confed.* **2022**, *187*, 110317.
15. Hou, Y.; Tan, Q.; Li, Q.; Song, Y.; Li, G. Measurement of the cam spacing on camshaft by binocular vision. *Int. J. Multimed. Ubiquitous Eng.* **2016**, *11*, 139–146.
16. Kiraci, E.; Palit, A.; Donnelly, M.; Attridge, A.; Williams, M.A. Comparison of in-line and off-line measurement systems using a calibrated industry representative artefact for automotive dimensional inspection. *Meas. J. Int. Meas. Confed.* **2020**, *163*, 108027.
17. Jeong, Y.; Lee, W.; Lee, K. Accuracy evaluation of dental models manufactured by CAD/CAM milling method and 3D printing method. *J. Adv. Prosthodont.* **2018**, *10*, 245–251.
18. Wang, S.; Wu, Z.; Peng, D.; Li, W.; Chen, S.; Liu, S. An angle displacement sensor using a simple gear. *Sensors Actuators A Phys.* **2018**, *270*, 245–25.
19. Li, S.; Zeng, L.; Feng, P.; Yu, D. An accurate probe pre-travel error compensation model for five-axis on-machine inspection system. *Precis. Eng.* **2020**, *62*, 256–264.
20. Stoup, J.; Doiron, T. A novel high accuracy micrometer for the measurement of diameter. *Metrologia.* **2021**, *58*, 025002.
21. Notabug.org: “Free Code Hosting”. Program That Helps in the Design Process of a Follower-Cam Mechanism. Available online: <https://notabug.org/anengineer/qtcam> (accessed on 4 May 2022).
22. Zayas Figueras, E.E. Aportación al Estudio de Levas Desmodrómicas. Ph.D. Thesis, Universitat Politècnica de Catalunya, (Barcelona Tech UPC), Barcelona, Spain, 2001.
23. Cimatech. Available online: <https://www.cimatech.com/productos/cimatron/cimatech-productos-cimatron.html> (accessed on 29 September 2022).
24. Buj, I.; Vivancos, J. and González, H. Influence of feed, eccentricity and helix angle on topography obtained in side milling processes. *Int. J. Mach. Tools Manuf.* **2011**, *51*, 889–897.
25. Buj-Corral, I.; Domínguez-Fernández, A.; Durán-Llucà, R. Influence of print orientation on surface roughness in fused deposition modeling (FDM) processes. *Materials* **2019**, *12*, 3834.
26. Buj-Corral, I.; Zayas-Figueras, E.E. Comparative study about dimensional accuracy and orm errors of FFF printed spur gears using PLA and Nylon. *Polymer Testing.* **2023**, *117*, 107862.
27. Beniak, J.; Križan, P.; Šooš, M.; Matuš, M. Research on Shape and Dimensional Accuracy of FDM Produced Parts. In Proceedings of the IOP Conference Series: Materials Science and Engineering, Phuket, Thailand, 11–14 December 2018.
28. Pennington, R.C.; Hoekstra, N.L.; Newcomer, J.L. Significant factors in the dimensional accuracy of fused deposition modelling. *J. Process Mech. Eng.* **2005**, *219*, 89–92.
29. Zharylkassyn, B.; Perveen, A.; Talamona, D. Effect of process parameters and materials on the dimensional accuracy of FDM parts. *Mater. Today Proc.* **2021**, *44*, 1307–1311.
30. Popescu, D.; Amza, C.G.; Marinescu, R.; Iacob, M.C.; Căruțașu, N.L. Investigations on Factors Affecting 3D-Printed Holes Dimensional Accuracy and Repeatability. *Appl. Sci.*, **2023**, *13*, 41.
31. Robthbart, H. Chapter 10: Cam Manufacturing. In *CAM DESIGN HANDBOOK: Cam Size and Profile Determination, Numerical Controls for Manufacturing, Computer Aided Design Techniques*; Rohtbart, H., Ed.; McGraw-Hill Companies: New York, NY, USA, 2004; pp. 285–296.
32. Buj-Corral, I.; Bagheri, A.; Sivatte-Adroer, M. Effect of Printing Parameters on Dimensional Error, Surface Roughness and Porosity of FFF Printed Parts with Grid Structure. *Polymers* **2021**, *13*, 1213.
33. Galantucci, L.M.; Lavecchia, F.; Percoco, G. Experimental study aiming to enhance the surface finish of fused deposition modeled parts. *CIRP Ann.* **2009**, *58*, 189–192.
34. Hartcher-O’Brien, J.; Evers, J.; Tempelman, E. Surface roughness of 3D printed materials: Comparing physical measurements and human perception. *Mater. Today Commun.* **2019**, *19*, 300–305.
35. Agulló, J.; Cardona, S. *Assessment of Surface Roughness (Valoración de la Rugosidad Superficial)*; Asociación Nacional de la Máquina—Herramienta: San Sebastián, Spain, 1974.



36. Norton, R. Cam materials and manufacturing. In *Cam Design and Manufacturing Handbook*; Norton, R., Ed.; Industrial Press Inc.: New York, NY, USA, 2009; Chapter 14, pp. 467–470.
37. Veera Ajay, C.; Pradeep, B.A.; Boopathi, C.; Sanjeev, R.K.; Meganathan, V. Comparison of geometrical accuracy and surface finish of cam profile generated by wire-EDM and CNC milling machine. In *Proceedings of the IOP Conference Series: Materials Science and Engineering*, Sathyamangalam, India, 10–11 September 2019.

**Disclaimer/Publisher's Note:** The statements, opinions and data contained in all publications are solely those of the individual author(s) and contributor(s) and not of MDPI and/or the editor(s). MDPI and/or the editor(s) disclaim responsibility for any injury to people or property resulting from any ideas, methods, instructions or products referred to in the content.